COLLECTIVE DYNAMICS AND FRAGMENTATION IN NUCLEAR SYSTEMS*

V. BARAN[1], M. MARCIU[1], D.I. PALADE[1], M. COLONNA[2],
M. DI TORO[2], A.I. NICOLIN[1,3], R. ZUS[1]

[1]Faculty of Physics, University of Bucharest, 405 Atomiştilor, POB MG-11, RO-077125,
Bucharest-Măgurele, România
[2]Laboratori Nazionali del Sud, INFN, 95123 Catania, Italy
[3]"Horia Hulubei" National Institute of Physics and Nuclear Engineering,
407 Atomiştilor, POB MG-6, RO-077125, Bucharest-Măgurele, România
E-mail: baran@nipne.ro

Received March 3, 2015

In this work we discuss different features of the collective dynamics in neutron rich nuclei which can contribute to constrain the dependence with density of the symmetry energy below saturation. As two components systems, they manifest both isoscalar and isovector modes whose stability is changing with density in a different manner. Within a Fermi liquid theory it is predicted that the isovector modes remain stable at densities under saturation while the isoscalar modes become unstable below a certain value of density. In connection to the former modes the electric dipole response of exotic nuclei shows the emergence of a low energy component when the number of neutrons in excess increases, which is associated to the dynamics of the low density neutron skin against a more stable core. Within schematic models which generalize the Brown-Bolsterli approach as well as in mean-field descriptions based on the Landau-Vlasov equation, we analyze the role of the symmetry energy on the energy centroid position and on the sum rules for this mode. Then, by considering the same parameterizations with density of the symmetry energy we investigate the isospin dynamics in the conditions when the growth of the unstable isoscalar fluctuations determine the nuclear fragmentation at Fermi energies.

Key words: Symmetry energy, Collective modes, Nuclear fragmentation.

PACS: 21.30.Fe, 24.10.Cn, 25.70.Ef.

1. INTRODUCTION

The symmetry energy term, $\frac{E_{sym}}{A}$, appearing in the nuclear Equation of State (EOS) in connection with the effects associated with the difference between the number of neutrons N and of protons Z is determined both by the Pauli correlations and by the properties of the nuclear interactions [1]. In the expression of the energy per nucleon $\frac{E}{A}(\rho, I)$

$$\frac{E}{A}(\rho, I) = \frac{E}{A}(\rho) + \frac{E_{sym}}{A}(\rho) I^2 \tag{1}$$

*Paper presented at the conference "Advanced many-body and statistical methods in mesoscopic systems II", September 1-5, 2014, Brasov, Romania.

it factorizes the square of the isospin degree of freedom $I = \frac{N-Z}{A}$ (here $\rho = \frac{A}{V}$ is the nuclear density and $A = N + Z$ is the mass number). For example, in a nuclear Energy Density Functional (EDF) approach derived from Skyrme-like interactions, the symmetry energy can decompose as follows:

$$\frac{E_{sym}}{A}(\rho) \equiv \epsilon_{sym} = \frac{E_F(\rho)}{3} + \frac{C(\rho)}{2}\frac{\rho}{\rho_0} = b_{sym}^{(kin)} + b_{sym}^{(pot)} \tag{2}$$

with E_F being the Fermi energy and $C(\rho)$ a function depending on the selected effective interaction. Several phenomena, such as the development of the neutron skin, the isovector collective response, the heavy ion dynamics and the isospin composition of the final products, as well as some essential processes in nuclear astrophysics depend on the behavior with density of this quantity [2, 3]. Within the EDF approach we proposed three parameterizations which give similar values of the symmetry energy E_{sym}/A at saturation density $\rho_0 = 0.16fm^{-3}$ but present quite different slopes around this point. For asystiff EOS, the coefficient $C(\rho)$ in (2) is constant, $C(\rho) = 32MeV$ and $\frac{E_{sym}}{A}(\rho_0) = 28.3MeV$. The slope parameter $L = 3\rho_0 \frac{dE_{sym}/A}{d\rho}|_{\rho=\rho_0}$ takes the value $L = 72MeV$. For the asysoft case we have $\frac{C(\rho)}{\rho_0} = (482 - 1638\rho)MeVfm^3$ which leads to a value $L = 14.4MeV$. Finally, for the asysuperstiff EOS, $\frac{C(\rho)}{\rho_0} = \frac{32}{\rho_0}\frac{2\rho}{(\rho+\rho_0)}$, the symmetry term has a faster variation around saturation density with a slope $L = 96.6MeV$. The corresponding nuclear mean-fields $U_q, (q = n, p)$, derived in this approach contain an isoscalar part expressed in terms of the nucleons density $\rho = \rho_n + \rho_p$ as well as an isovector part that depend on isovector density $\rho_i = \rho_n - \rho_p$ and is determined by $C(\rho)$

$$U_q(\mathbf{r}) = A\frac{\rho}{\rho_0} + B(\frac{\rho}{\rho_0})^{\alpha+1} + C(\rho)\frac{\rho_n - \rho_p}{\rho_0}\tau_q + \frac{1}{2}\frac{\partial C}{\partial \rho}\frac{(\rho_n - \rho_p)^2}{\rho_0} \quad . \tag{3}$$

Here $\rho_n(\mathbf{r})$ ($\rho_p(\mathbf{r})$) is the neutron (proton) local density and $\tau_n(\tau_p) = +1(-1)$. The coefficient A, B and the exponent α are selected in order to reproduce the features of nuclear matter at saturation.

In this work we present results concerning the effects of the density dependence of symmetry energy below saturation derived in transport approaches based on Landau-Vlasov equation [4] and in schematic models [5]. We focus both on the properties of the isovector-like modes, which remain stable even for dilute systems was well as on those of isoscalar-like modes which below a certain value of density become unstable [6]. Indeed, let us observe that (3) represents one of the main ingredients in the Landau-Vlasov equations for one-body distributions functions of

protons and neutrons:

$$\frac{\partial f_p}{\partial t} + \frac{\mathbf{p}}{m} \cdot \nabla_{\mathbf{r}} f_p - \nabla_{\mathbf{r}} U_p \cdot \nabla_{\mathbf{p}} f_p \quad = I(f_p, f_n)\,, \tag{4}$$

$$\frac{\partial f_n}{\partial t} + \frac{\mathbf{p}}{m} \cdot \nabla_{\mathbf{r}} f_n - \nabla_{\mathbf{r}} U_n \cdot \nabla_{\mathbf{p}} f_n \quad = I(f_p, f_n)\,. \tag{5}$$

When the collision integral $I(f_p, f_n)$ is neglected (4) and (5) reduce to two coupled Vlasov equations representing the semiclassical limit of Time Dependent Hartree Fock (TDHF) approximation and which in the linear regime can be related to the Random Phase Approximation (RPA). Similarly, within the Brown-Bolsterli schematic model [7, 8], the interaction $A_{ij} = \bar{V}_{ph'hp'} = V_{ph',hp'} - V_{ph',p'h} = \langle ph'|\hat{V}|hp'\rangle - \langle ph'|\hat{V}|p'h\rangle$ is approximated (neglecting the exchange term) by a separable particle-hole interaction $A_{ij} = \lambda D_{ph} D^*_{p'h'} = \lambda Q_i Q^*_j$ whose coupling constant depends on the potential symmetry energy term $b^{(pot)}_{sym}$ at normal density, $\lambda(\rho_0) = \dfrac{6 b^{(pot)}_{sym}(\rho_0)}{A\langle r^2\rangle}$ [9]. In these expressions *i* define an specific particle-hole *ph* pair, D_{ph} refers to the corresponding matrix elements of the dipole operator while $\langle r^2\rangle$ is the mean square radius of the nucleus. With this value for λ and accounting for the sum-rules satisfied by the matrix elements $|Q_i|^2$ [10], the energy centroid and the EWSR exhausted by the GDR were successfully reproduced by the RPA treatment.

In the next section we explore the emergence of Pygmy Dipole Resonance in neutron rich nuclei within the models mentioned above and look at the role of the symmetry energy on the position of the energy centroid of this mode as well on the associated Energy Weighted Sum Rule (EWSR). Then, by employing the same parameterizations with density of the symmetry energy we explore the fragmentation dynamics in connection with isospin dynamics within the Stochastic Mean Field (SMF) model [11].

2. PYGMY DIPOLE RESONANCE: FROM SCHEMATIC MODELS TO TRANSPORT APPROACHES

Finite nuclei and particularly neutron-rich systems exhibit a well defined density profile with several neutrons located in a region at lower density forming the neutron skin. Since the symmetry energy decreases with density in a schematic Brown-Bolsterli approach one expects for the nucleons located in the surface region to be associated a separable interaction with a value of the coupling constant smaller than $\lambda(\rho_0)$. Similar arguments can be found in phenomenological models [12] when three coupled fluids (*i.e.*, protons, blocked neutrons and excess neutrons) were proposed to define the normal modes in a hydrodynamical description. Therefore in the schematic approach we relax the condition of a unique coupling constant for all

particle-hole pairs. Such more general separable interactions were considered also in a microscopic model aiming to include the coupling between normal and threshold states [13] or to study the GDR in fissioning nuclei [14]. We assume that for a subsystem of particle-hole pairs, namely $i,j \leq i_c$, the interaction is $A_{ij} = \lambda_1 Q_i Q_j^*$, with $\lambda_1 = \lambda(\rho_0)$ corresponding to the potential symmetry energy at saturation density, while for the other subsystem, namely $i,j > i_c$, the interaction is characterized by a weaker strength $A_{ij} = \lambda_3 Q_i Q_j^*$, with $\lambda_3 = \lambda(\rho_e)$ associated with the symmetry energy value at a much lower density $\rho_e << \rho_0$. If $i \leq i_c, j > i_c$ or $i > i_c, j \leq i_c$, *i.e.*, for the coupling between the two subsystems, we consider $A_{ij} = \lambda_2 Q_i Q_j^*$ with $\lambda_2 = \lambda(\rho_i)$ corresponding to a potential symmetry energy at an intermediate density $\rho_0 > \rho_i > \rho_e$ and consequently $\lambda_1 > \lambda_2 > \lambda_3 > 0$. The RPA equations for the forward and backward amplitudes $X_i^{(n)}, Y_i^{(n)}$ become

$$\epsilon_i X_i^{(n)} + \lambda_1 Q_i \sum_{j \leq i_c} (Q_j^* X_j^{(n)} + Q_j Y_j^{(n)}) + \lambda_2 Q_i \sum_{j > i_c} (Q_j^* X_j^{(n)} + Q_j Y_j^{(n)}) = E_n X_i^{(n)}$$

$$\epsilon_i Y_i^{(n)} + \lambda_1 Q_i^* \sum_{j \leq i_c} (Q_j^* X_j^{(n)} + Q_j Y_j^{(n)}) + \lambda_2 Q_i^* \sum_{j > i_c} (Q_j^* X_j^{(n)} + Q_j Y_j^{(n)}) = -E_n Y_i^{(n)}$$

if $i \leq i_c$,

$$\epsilon_i X_i^{(n)} + \lambda_2 Q_i \sum_{j \leq i_c} (Q_j^* X_j^{(n)} + Q_j Y_j^{(n)}) + \lambda_3 Q_i \sum_{j > i_c} (Q_j^* X_j^{(n)} + Q_j Y_j^{(n)}) = E_n X_i^{(n)}$$

$$\epsilon_i Y_i^{(n)} + \lambda_2 Q_i^* \sum_{j \leq i_c} (Q_j^* X_j^{(n)} + Q_j Y_j^{(n)}) + \lambda_3 Q_i^* \sum_{j > i_c} (Q_j^* X_j^{(n)} + Q_j Y_j^{(n)}) = -E_n Y_i^{(n)}$$

if $i > i_c$.

From these equations, with $\alpha = \sum_{i \leq i_c} |Q_i|^2$, $\beta = \sum_{i > i_c} |Q_i|^2$, in the degenerate case $\epsilon_i = \epsilon$ are obtained the following collective RPA energies:

$$E_{n,RPA}^{(1)2} = \epsilon^2 + 2\epsilon(E_{n,TDA}^{(1)} - \epsilon) = \epsilon(2E_{n,TDA}^{(1)} - \epsilon), \tag{6}$$

$$E_{n,RPA}^{(2)2} = \epsilon^2 + 2\epsilon(E_{n,TDA}^{(2)} - \epsilon) = \epsilon(2E_{n,TDA}^{(2)} - \epsilon), \tag{7}$$

where $E_{n,TDA}^{(1)}$ and $E_{n,TDA}^{(2)}$ are the corresponding energies in the TDA approximation

$$E_{n,TDA}^{(1)} = \epsilon + \frac{(\lambda_1\alpha + \lambda_3\beta)}{2}\left(1 + \sqrt{1 - \frac{4(\lambda_1\lambda_3 - \lambda_2^2)\alpha\beta}{(\lambda_1\alpha + \lambda_3\beta)^2}}\right) \tag{8}$$

$$E_{n,TDA}^{(2)} = \epsilon + \frac{(\lambda_1\alpha + \lambda_3\beta)}{2}\left(1 - \sqrt{1 - \frac{4(\lambda_1\lambda_3 - \lambda_2^2)\alpha\beta}{(\lambda_1\alpha + \lambda_3\beta)^2}}\right). \tag{9}$$

From the EWSR for the unperturbed system is obtained that $m_1 = \hbar\omega_0(\alpha +$

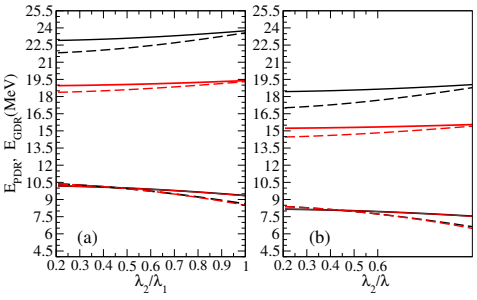

Fig. 1 – (Color on-line) The GDR and PDR energy centroids as a function of the ratio λ_2/λ_1. The black thick lines refer to the TDA while the red lines to RPA calculations. (a) For ^{68}Ni the solid lines correspond to $N_e = 6$; the dashed lines correspond to $N_e = 12$. (b) For ^{132}Sn the solid lines correspond to $N_e = 12$; the dashed lines correspond to $N_e = 32$.

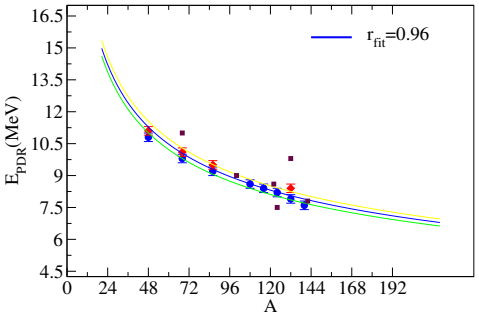

Fig. 2 – (Color on-line) The mass dependence of the PDR energy centroid as a function of mass predicted by the transport model (blue circles and red diamonds). The three lines of fit corresponds to the mass parameterizations $40A^{-1/3}, 41A^{-1/3}$ and $42A^{-1/3}$. The maroon squares represent experimental data points, see [18].

$\beta) = \dfrac{\hbar^2}{2m}\dfrac{NZ}{A}$. The specific values for α and β are connected to the number of protons (Z_c) and neutrons (N_c) which belong to core, ($A_c = N_c + Z_c$) and the number of neutrons in excess, *i.e.* nucleons at lower density (N_e), respectively. Then results $\hbar\omega_0\alpha = \dfrac{\hbar^2}{2m}\dfrac{N_c Z}{A_c}$ and $\hbar\omega_0\beta = \dfrac{\hbar^2}{2m}\dfrac{N_e Z^2}{AA_c}$ [15, 16]. Since in the presence of the dipolar field the charges of protons and neutrons are N/A and $-Z/A$, respectively. The coupling constant will become $\lambda_1 = \dfrac{A^2}{NZ}\dfrac{10 b_{sym}^{(pot)}(\rho_0)}{AR^2}$, where the nuclear radius is $R = 1.2A^{1/3}$. We adopt for λ_3 a value $\lambda_3 = 0.2\lambda_1$ corresponding to the lower density associated with the neutron skin region. Then λ_2 is varied from λ_3 *i.e.* a weak coupling between the two subsystems to λ_1 *i.e.* a strong coupling between the two subsystems. We selected for the study the systems ^{68}Ni and ^{132}Sn. For these conditions in Fig. 1 (a),(b) we report the position of the energy centroids of the two collective states both in TDA (black thick lines) and RPA (red lines) calculations. For ^{68}Ni the number of neutrons in excess is $N_e = 12$ (dashed lines) and $N_e = 6$ (solid lines) respectively. The PDR energy centroid does not change much when we modify the value of N_e. The experimental value is $E_{PDR}^{exp} = 9.55$ MeV [17], while in our calculations for $N_e = 6$, it varies from $E_{PDR} = 10.2$ MeV to 9.3 MeV, when λ_2 increases. In the case of ^{132}Sn we chose $N_e = 32$ (dashed lines) and $N_e = 12$ (solid lines). For $N_e = 12$ the position of the PDR energy centroid changes from $E_{PDR} = 8.5$ MeV to 7.5 MeV as λ_2 is varied between the same limits. In Fig. 2 we report the mass dependence of E_{PDR} as predicted by the model based on Vlasov

Table 1

The ratios λ_2/λ_1, λ_3/λ_1 corresponding to the realistic physical conditions for the three asy-EOS, the predicted values of PDR, E_{PDR} and GDR, E_{GDR}, energy centroids (in MeV), the fraction f_{PDR} exhausted by the PDR in each case. f^V_{PDR} refers to the values obtained from Vlasov calculations.

asy-EoS	λ_2/λ_1	λ_3/λ_1	E_{PDR}	E_{GDR}	$f_{PDR}(\%)$	$f^V_{PDR}(\%)$
asysoft	0.57	0.23	7.98	15.30	1.3	2.4
asystiff	0.31	0.11	8.05	15.20	3.3	4.2
asysupstiff	0.15	0.02	8.05	15.17	5.0	4.4

equations [18]. From a direct comparison is concluded that for the two systems the agreement between the two models is very good.

Therefore we extend the comparison and analyze the role of the symmetry energy. Few additional assumptions concerning the connection between the values of λ_i in the schematic model and the density behavior of the symmetry energy are considered. We employ the three mentioned parameterizations of the potential symmetry energy and determine for each of them the ratio of the coupling constant at a given density ρ to the coupling constant at the saturation density, $\lambda(\rho)/\lambda(\rho_0)$. We focus the analysis on ^{132}Sn and approximate the radial proton and neutron density distributions by trapezoidal shapes [19]. The proton mean-square radius is well reproduced and obtain a neutron skin thickness $\Delta R_{np} = 0.3fm$ when we adopt for the central densities the values provided by the Vlasov calculations [16], $\rho_n = 0.0825fm^{-3}, \rho_p = 0.0575fm^{-3}$ [5]. We consider the number of neutrons in excess as being determined by the neutron density distribution beyond $r = 6.5$ fm, where the tail of the protons distribution is approaching the end part. In this way we obtain a value of N_e around 13.5 neutrons. We also assume that the average density of these particles will define ρ_e, obtaining $\rho_e = 0.0186fm^{-3}$. For the three asy-EOS the ratio $\lambda_3/\lambda_1 = \lambda(\rho_e)/\lambda(\rho_0)$ ratio is shown in Table 1. We assume that the properties of the region where the total density changes from ρ_0 to zero determine the coupling between the core and the excess neutrons. The average density of this region will correspond to ρ_i. The obtained value is $\rho_i = 0.05fm^{-3}$. For the three asy-EOS the calculated ratio $\lambda_2/\lambda_1 = \lambda(\rho_i)/\lambda(\rho_0)$ is reported in Table 1. With these values of the parameters the PDR energy is found around 8 MeV in all cases. The EWSR fraction f_{PDR} exhausted by PDR is strongly influenced by the density dependence of the symmetry energy below saturation. When we pass from the asysoft to the superasystiff its values are 1.3%, 3.3% and 5.0%. Moreover this trend is consistent with the predictions of the transport model, see Table 1, where again a similar increase of the EWSR fraction with the slope parameter L can be noticed. Taking into account the approximations present in each model the overall agreement is quite good, providing a clear evidence of the relation between the behavior of the symmetry energy at lower

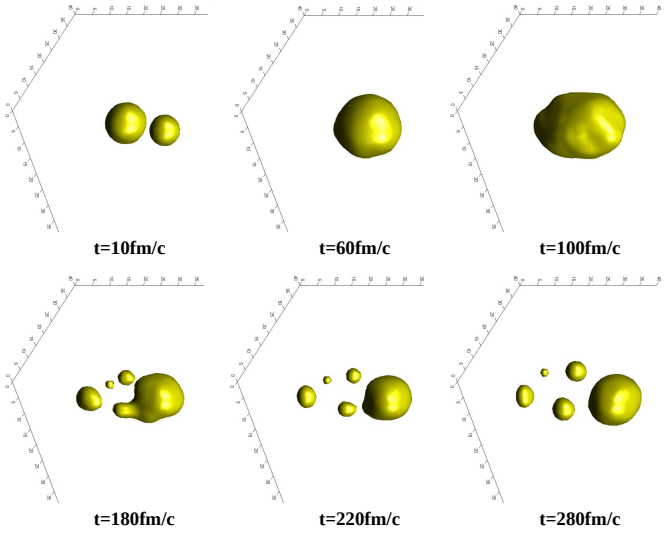

Fig. 3 – (color on-line) The time evolution of a fragmentation event following the collision ^{124}Sn+^{68}Ni at 45A·MeV and impact parameter $b = 3fm$.

densities and the PDR response.

3. ISOSPIN DYNAMICS IN NECK FRAGMENTATION

In this section we adopt a transport model based on Landau-Vlasov equations, the Stochastic Mean Field, which includes a method to account for the effects of fluctuations through a projection in real space [11]. The approach is appropriate to explore unstable regimes of nuclear matter as in the case of spinodal decomposition. This represents one of the kinetic mechanisms which leads to nuclear fragmentation in collisions at intermediate energies through exponential amplification of the initial density fluctuations. The possible correlations between the kinematic properties of the Intermediate Mass Fragments (IMF's) and their isospin content which add new constrains on the behavior with density of symmetry energy stimulated more exclusive experiments [20–24] as well as theoretical investigations [25–28]. Here we present features of the neck fragmentation mechanism for the CHIMERA system ^{124}Sn+^{68}Ni and of the dynamics of isospin degree of freedom for this reaction.

In Fig. 3 we depict the time evolution following the collision at 45A·MeV beam energy and impact parameter $b = 3fm$. Already at this centrality zone the coexistence of different fragment production mechanisms manifests. After an expansion stage first IMF's are growing in the low density region. Then, on longer time scales, after $180fm/c$ in this example, the dynamically induced fission of PLF-like

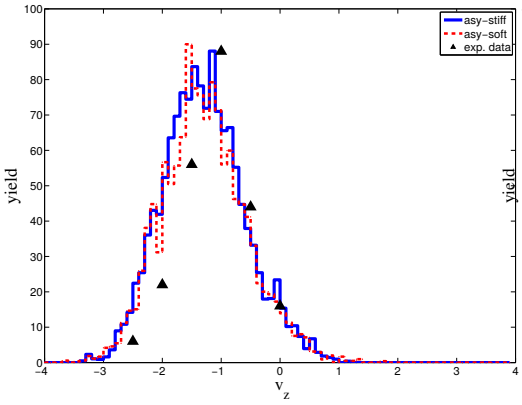

Fig. 4 – (color on-line) Parallel velocity distribution (in cm/ns) of the IMF's with$Z = 4$ produced in ternary events. The black triangles refer to experimental data points. In order to perform the comparison the theoretical predictions were normalized to data at $v_z = 0.0$ cm/ns.

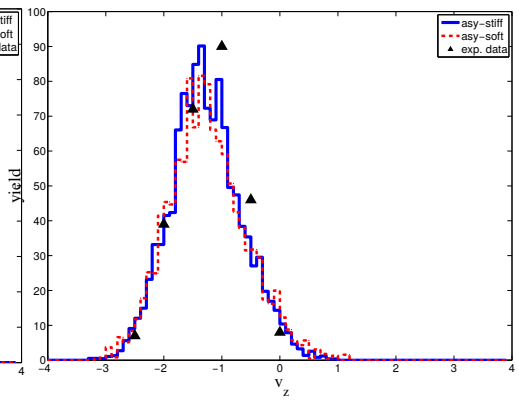

Fig. 5 – Parallel velocity distribution of the IMF's with charge $Z = 5$ produced in ternary events). The black triangles refer to experimental data points. In order to perform the comparison the theoretical predictions were normalized to data at $v_z = 0.0$ cm/ns.

system can also takes place. The model is able to reproduce nicely several kinematic properties observed experimentally. In Fig. 4 and Fig. 5 we present a comparison with data of parallel velocity distribution for IMF's with $Z = 4$ and $Z = 5$.

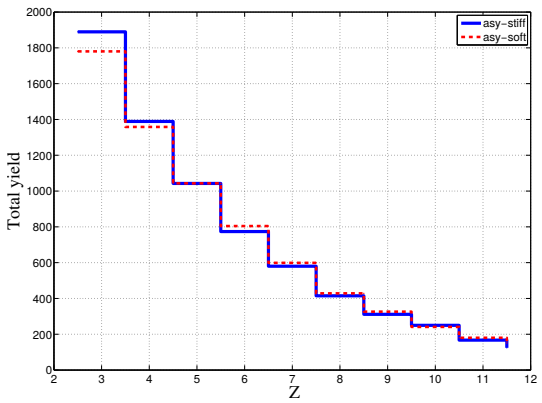

Fig. 6 – The IMF charge distribution for the ternary events of the reaction ^{124}Sn+^{64}Ni at 45AMeV.

The charge distribution of IMF's produced in the ternary fragmentation events is represented in Fig. 6 for asy-stiff and asy-soft EOS. We cannot distinguish differences between the two asy-EOS. One reason is that for semicentral to semiperipheral collisions the fragment formation and growth is mainly determined by the competition between the isoscalar-like bulk instabilities and surface instabilities. However the isospin content of the primary IMF's is quite different for the two asy-EOS as is shown in Fig. 7 and Fig. 8 where the average value of N/Z was plotted as a function the fragments charges. Moreover, we also observed, following a more detailed analy-

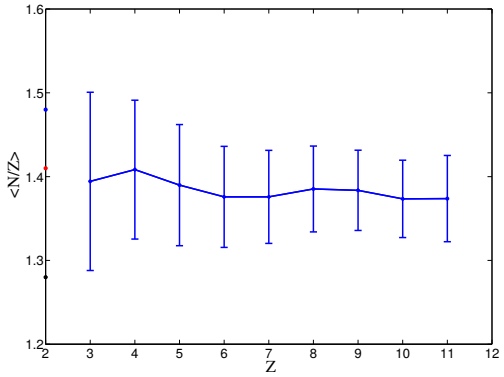

Fig. 7 – (Color on-line) The IMF's average value of N/Z as a function of charge Z. The asystiff EOS.

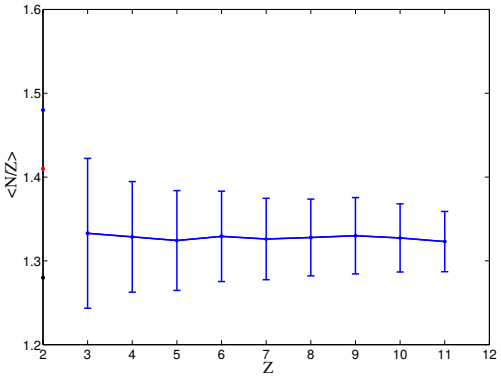

Fig. 8 – (Color on-line) The IMF's average value of N/Z as a function of charge Z. The asysoft EOS.

sis, that the isospin content distribution as a function of various kinematic quantities including transverse velocity and deviation from Viola systematics are sensitive to the fragmentation mechanism and the production time scale. These results will be reported soon once the analysis will be completed for all asyEOS [29].

4. CONCLUSIONS

In this work we have studied several observables which are influenced by the symmetry energy behavior below saturation density. In order to account for the density dependence of the symmetry energy within the Brown-Bolsterli models based on separable interactions, the condition of a unique coupling constant for all particle-hole interactions was relaxed. The coupling constants for the isovector dipole response are related to the potential part of the symmetry energy and the obtained model is appropriate to describe situations when part of the nucleons are located in a region at lower density, as is the neutron skin. In this case we find that the coherent superposition of particle-hole states generate two collective states sharing all the EWSR. For realistic values of the parameters, we reproduce simultaneously the basic ex-

perimental features of GDR and PDR. The results concerning the role of the low density behavior of symmetry energy on the EWSR exhausted by PDR are consistent with the predictions based on self-consistent transport models when in the isovector sector of EOS are considered the same effective interactions. Precise experimental determinations of the properties of the low energy dipole response can add important constraints on the behavior of the symmetry energy well below saturation. At Fermi energies we shown that the specific correlations between kinematic observables and isospin content of the IMF's are also influenced by the dependence with density of the symmetry energy and more exclusive fragmentation experiments will provide essential information about this quantity below saturation.

Acknowledgements. This work for V. Baran, R. Zus and A.I. Nicolin has been supported by the project from the Romanian National Authority for Scientific Research, CNCS-UEFISCDI, project number PN-II-ID-PCE-2011-3-0972. M. Marciu was supported by the strategic grant POSDRU/159/1.5/S/137750, "Project Doctoral and Postdoctoral programs support for increased competitiveness in Exact Sciences research" co-financed by the European Social Found within the Sectorial Operational Program Human Resources Development 2007-2013. A. I. Nicolin was also supported by PN 09370108/2015.

REFERENCES

1. V. Baran, M. Colonna, M. Di Toro, V. Greco, *Phys. Rep.* **410**, 335 (2005).
2. A.W. Steiner, M. Prakash, J.M. Lattimer, P. Ellis, *Phys. Rep.* **411**, 325 (2005).
3. Li Bao-An, Lie-Wen Chen, Che Ming Ko, *Phys. Rep.* **464**, 113 (2008).
4. V. Baran, M. Colonna, M. Di Toro, B. Frecus, A. Croitoru, D. Dumitru, *Eur. Phys. J.* D **68**, 356 (2014).
5. V. Baran, D.I. Palade, M. Colonna, M. Di Toro, A. Croitoru, A. I. Nicolin, *Phys. Rev.* C **91**, 054303 (2015).
6. V. Baran, M. Colonna, M Di Toro, V. Greco, *Phys. Rev. Lett.* **86**, 4492 (2001).
7. G.E. Brown, M. Bolsterli, Phys. Rev. Lett. **3**, 472 (1959).
8. G.E. Brown, J.A. Evans, D.J. Thouless, Nucl. Phys. A **24**, 1 (1961).
9. A. Bohr, B. R. Mottelson, *Nuclear Structure* vol II, p. 481 (World Scientific, Singapore, 1998).
10. P. Ring and P. Schuck *The Nuclear Many Body Problem* (Springer-Verlag, New York-Berlin, 1980).
11. V. Baran, M. Colonna, M. Di Toro, V. Greco, M. Zielinska-Pfabe, H. H. Wolter, *Nucl. Phys.* A **703**, 603 (2002).
12. R. Mohan, M. Danos, L.C. Biedenharn, *Phys. Rev.* **3**, 1740 (1971).
13. H.W. Barz, L.P. Csernai, *Nucl. Phys.* A **340**, 143 (1980).
14. P.-G. Reinhard, D. Drechsel, *Nucl. Phys.* A **295**, 125 (1978).
15. V.Baran *et al.*, *Rom. J. Phys.* **57**, 36 (2012).
16. V. Baran, B. Frecus, M. Colonna, M Di Toro, *Phys. Rev.* C **85**, 051601(R) (2012).
17. D.M. Rossi *et al.*, Phys. Rev. Lett. **111**, 242503 (2013).
18. V. Baran, M. Colonna, M Di Toro, A. Croitoru, D. Dumitru, *Phys. Rev.* C **88**, 044610 (2013).
19. T. Ikehara, M. Yamada, *Prog. Theor. Phys.* **71**, 1254 (1984).
20. E. De Filippo *et al.*, *Phys. Rev.* C **71**, 044602 (2005).

21. E. De Filippo *et al.*, *Phys. Rev.* C **86**, 014610 (2012).
22. S. Hudan *et al.*, *Phys. Rev.* C **86**, 021603 (2012).
23. K. Brown *et al.*, *Phys. Rev.* C **87**, 061601 (2013).
24. P. Russotto *et al.*, *Phys. Rev.* C **91**, 014610 (2015).
25. V. Baran, M. Colonna, M. Di Toro, *Nucl. Phys.* A **340**, 143 (2004).
26. R. Lionti, V. Baran, M. Colonna, M. Di Toro, *Phys. Lett.* B **625**, 33 (2005).
27. M. Papa *et al.*, *Phys. Rev.* C **88**, 044610 (2012).
28. V. Baran, M. Colonna, M Di Toro, R. Zus *Phys. Rev.* C **88**, 044610 (2012).
29. M. Marciu *et al.*, to be submitted for publication.